



Effects of position and gap orientation of the split ring resonator structure excited by microstrip transmission line on the transmission characteristics

Nezihe KARACAN¹, Neslihan Kader BULUT², Evren EKMEKÇİ^{1,2,*}

¹Department of Electrical and Electronics Engineering, Faculty of Engineering,
Süleyman Demirel University, Isparta, Turkey

²Department of Electronics and Communication Engineering, Faculty of Engineering,
Süleyman Demirel University, Isparta, Turkey

Received: 20.11.2021

Accepted/Published Online: 08.10.2022

Final Version: 28.11.2022

Abstract: In this study, the effects of the position and the gap orientation of the split ring resonator (SRR) structure, which is applied as a superstrate, on transmission characteristics (i.e. $|S_{21}|$) are investigated numerically and experimentally. For that purpose, the left edge of the transmission line has been designated as the reference line and the SRR structure is shifted towards both left and right for three different gap orientations. Subsequently, $|S_{21}|$ characteristics of the SRR structure having several substrate thicknesses and several substrate dielectric constants are investigated parametrically for three different gap orientations. The results reveal that the position and the gap orientation of the SRR structure have effects on the amplitude and the resonance frequency observed in S_{21} . Moreover, it has been observed that the substrate thickness and the dielectric constant of the loaded SRR have significant effects on S_{21} in terms of amplitude and the resonance frequency. Lastly, transmission, reflection, and power distribution plots together with radiation patterns are investigated for three gap orientation cases to reveal power distribution mechanism. In general, this study verifies the literature, combine the analyses as a whole for fairer comparison due to the fact that the analyses have been concerned on the same characterization setup, and fill the gaps by completing the missing analyses. This comprehensive study is believed to be a useful guide for researchers in their studies conducted on sensor and filter designs.

Key words: Split ring resonator, microstrip transmission line, resonator loaded transmission line, transmission characteristics, split ring resonator position, split ring resonator gap orientation

1. Introduction

Metamaterials are artificial structures that present negative electrical permittivity and negative magnetic permeability [1]. The commonly used resonator structure in metamaterial designs, the split ring resonator (SRR), was proposed by Pendry et al. in the late 20th century [2]. The SRR is currently a popular structure that is used in sensor [3–11], filter [12–14], absorber [15, 16], electromagnetic induced transparency [17, 18], antenna [19, 20], and other applications. It is commonly excited by microstrip transmission lines (MSTL) in sensing [3–11] and filtering [12–14] applications.

The position and the gap orientation of the SRR with respect to the transmission line are important parameters that affect transmission characteristics (i.e. $|S_{21}|$) [13, 21–24]. In the literature, the position

*Correspondence: evrenmekci@sdu.edu.tr

[13, 21, 22] and the gap orientation [23, 24] of the SRR with respect to the transmission line on transmission characteristics were investigated in separate studies.

In this study, an SRR loaded MSTL configuration was studied to investigate the effects of the position, the gap orientation, and the substrate thickness of the SRR on the transmission characteristics on the same characterization setup in whole with additional and detailed parametric analyses. To investigate the SRR position with respect to the MSTL on transmission spectrum, the analyses were conducted for two different shift directions (i.e. shift to the left and shift to the right relative to MSTL). The position analyses were repeated for three different gap orientations of the SRR in simulations and in experiments. Subsequently, the effects of SRR substrate thickness and dielectric constant on transmission characteristics, while keeping the SRR position as constant, were investigated for several substrate thicknesses and three different gap orientations in simulations. In addition, the SRR sensitivities on the dielectric constants of dielectric loadings were investigated in a comparative manner for three different gap orientations. Lastly, transmission, reflection, and power distribution plots are investigated together with radiation patterns for three gap orientation cases to figure out power distribution mechanism.

As the contributions to the existing studies in the literature, in this study, the position and the gap orientation of the SRR structure were investigated together in whole and the effect of SRR substrate thickness and substrate dielectric constant on the transmission characteristics were investigated in detail for three different gap orientations. Besides, the effects of gap orientations on the sensitivity were studied for sensing applications. Finally, the power distribution mechanism was discussed in terms of the delivered power to the ports, the dissipated power in the structure, and the radiated power.

The preliminary results of this study has already been published as a national conference paper in Turkish [25]. This study presents significant extensions including additional analyses and discussions.

2. Design

The schematical views and the design parameters of the designed MSTL and the SRR, which is placed as a superstrate on MSTL, are shown in Figure 1a. The MSTL is composed of three layers; a copper ground at the bottom, a dielectric substrate in the middle, and a copper transmission line at the top. An FR4 type dielectric substrate material was used in common for the MSTL and the SRR at the first stage. Note that the dielectric constant of the SRR substrate (ϵ_r) and its height (h_r) were set as variables for further parametric analyses. The copper ($\sigma_{cu} = 5.8 \times 10^7$ S/m) and the dielectric thicknesses were defined as $t = 0.035$ mm and $h = h_r = 1.5$ mm, respectively. The dielectric properties of the substrate were retrieved by the implementation of Nicolson-Ross-Weir method [26, 27] in our laboratory by using S-parameters measurements and the properties were determined to be $\epsilon_r = \epsilon_{rt} = 4.53$ and $\tan \delta = 0.01$ at 3.7 GHz. The MSTL sizes were designed as $L_x \times L_y = 80 \times 100$ mm². The copper line width w_f were calculated to be 2.75 mm for 50 Ω characteristic impedance by using CST Studio Suite^{®1} impedance calculation tool; however, it was modelled as $w_f = 2.87$ mm (corresponds to approximately 49 Ω characteristic impedance) in simulations, since the fabricated MSTL had $w_f = 2.87$ mm line width due to fabrication errors. The square-shaped SRR had metallic side length $l_s = 9.2$ mm, line width $w_s = 1.1$ mm, gap with $g = 1$ mm, square-shaped SRR substrate side length $L_s = 11$ mm, and substrate height $h_r = 1.5$ mm. The parameter ϕ presented in Figure 1a was used to define the gap orientation and it took three values from 0° to 180° with a 90° step-size in counter-clockwise direction. To define the position of

¹CST STUDIO SUITE[®], Dassault Systèmes, the 3DEXPERIENCE[®] Company (online). Website www.3ds.com/products-services/simulia/products/cst-studio-suite/ [accessed 30 December 2021].

the SRR on MSTL, s and s_r parameters were defined as shown in Figure 1a. The photograph of the fabricated structures is shown in Figure 1b. The black dots in the photograph (on the right of the SRR) are a scale to position the SRR, composed with 1 mm step width. During the simulations and experiments, the left edge of the w_f -thick copper line was defined as the reference line (0 mm line). The SRR structure was shifted to left with s and shifted to right with s_r parameters to observe the effects on $|S_{21}|$ characteristics. While shifting towards the right, the SRR structure was lifted up to as much as the transmission line thickness (t) in simulations to avoid coincidence of the SRR structure with the metallic transmission line. In the design, the SRR and the MSTL were fabricated separately (i.e. in different layers), and no adhesive material was used in between them since both structures had planar interfaces and the final design was placed parallel to the earth's crust. The fabrication of the SRR on a different layer compared to the MSTL allowed all investigations (i.e. all shifting cases including three different gap orientations) possible with a single production. However, coplanar designs were also studied in simulations to complete the picture and provide a comparison. All investigations were conducted on the fundamental resonance mode of the SRR.

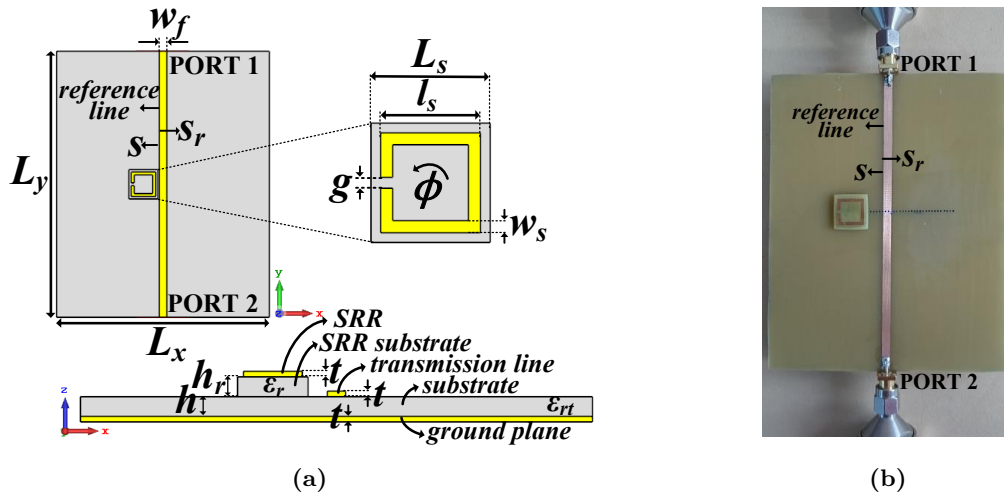


Figure 1. Microstrip transmission line (MSTL) and SRR structure. (a) Schematic views and the design parameters. (b) A photograph of SRR-loaded MSTL from the top view.

3. Simulations and experiments

The designs and the numerical analyses were conducted by commercial CST Studio Suite[®] software frequency domain solver. The simulation setup is shown in Figure 2. During the simulations, the space surrounding the structure was terminated by open boundary conditions and MSTL was excited by two waveguide ports at each end. The dimensions of the waveguide ports were determined and automatically constructed by the “calculate port extension coefficient” tool of CST Studio Suite[®]. For quasitransverse electromagnetic (quasi-TEM) mode propagation, the wave vector \vec{k} , the electric field vector \vec{E} , and the magnetic field vector \vec{H} are along $-y$ -, z -, and $-x$ - axes, respectively [28].

For the experimental measurements, MSTL was terminated by 50 Ω SMA type connectors at each end as shown in Figure 1b. The excitation of the MSTL and S -parameter measurements were performed by Agilent FieldFox N9926A vector network analyzer. The network analyzer was calibrated by SOLT (short-open-load-thru) calibration technique before the measurements.

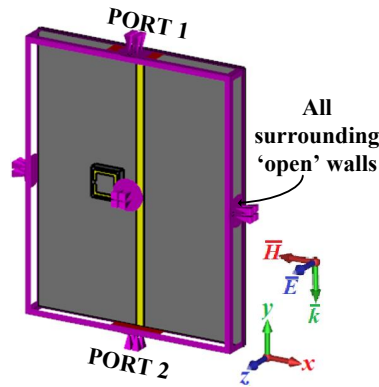


Figure 2. The simulation setup for the SRR-loaded MSTL.

4. Results

Firstly, $|S_{11}|$ (reflection) and $|S_{21}|$ (transmission) graphs for unloaded (i.e. SRR not deployed) MSTL were obtained for both simulations and experiments. The results are shown in Figure 3. The reflection coefficient is observed to be almost below -25 dB for all frequencies under interest. On the other hand, the transmission is around -1 dB level, which is assumed to be due to the use of a relatively lossy substrate. The experiments agree well with the simulations.

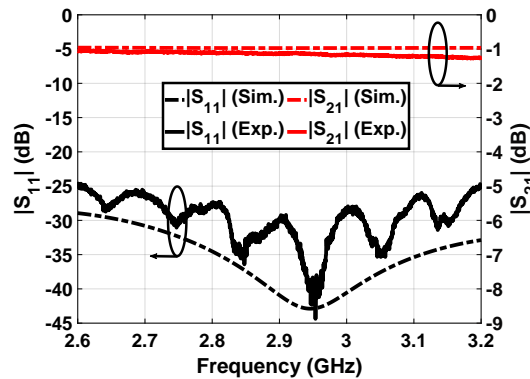


Figure 3. $|S_{11}|$ and $|S_{21}|$ plots of the unloaded MSTL obtained by simulations and experiments.

Subsequently, the effects of the position of the SRR with respect to the MSTL on $|S_{21}|$ characteristics were investigated for three different gap orientations. Firstly, the SRR was shifted to the left by using the parameter s , where it was changed from $s = 0$ mm to 5 mm with 1 mm steps. Herein, the parameter s specifies the distance between the reference line and the SRR as depicted in Figures 1 and 4. The corresponding simulation and experiment results are shown in Figure 4. The results reveal that as s increases, corresponding $|S_{21}|$ value observed at the f_0 resonance frequency (i.e. the frequency which $|S_{21}|$ makes a dip) increases for each gap orientation. Moreover, the resonance strength obtained for each s value decreases as ϕ tends to increase to 180° from 0° . It has been figured out that the decrease in the resonance strength depending on the increase in s is due to the decrease in the coupling between the SRR and the transmission line. As it can be observed in Figures 4e and 4f, for $\phi = 180^\circ$ case, no resonance is observed in simulations and experiments for $s = 3$ mm and beyond; therefore, $|S_{21}|$ plots are almost overlapped. In addition to that, f_0 shifts to the left for $\phi = 0^\circ$ case and shifts to the right for $\phi = 90^\circ$ and $\phi = 180^\circ$ cases as s increases.

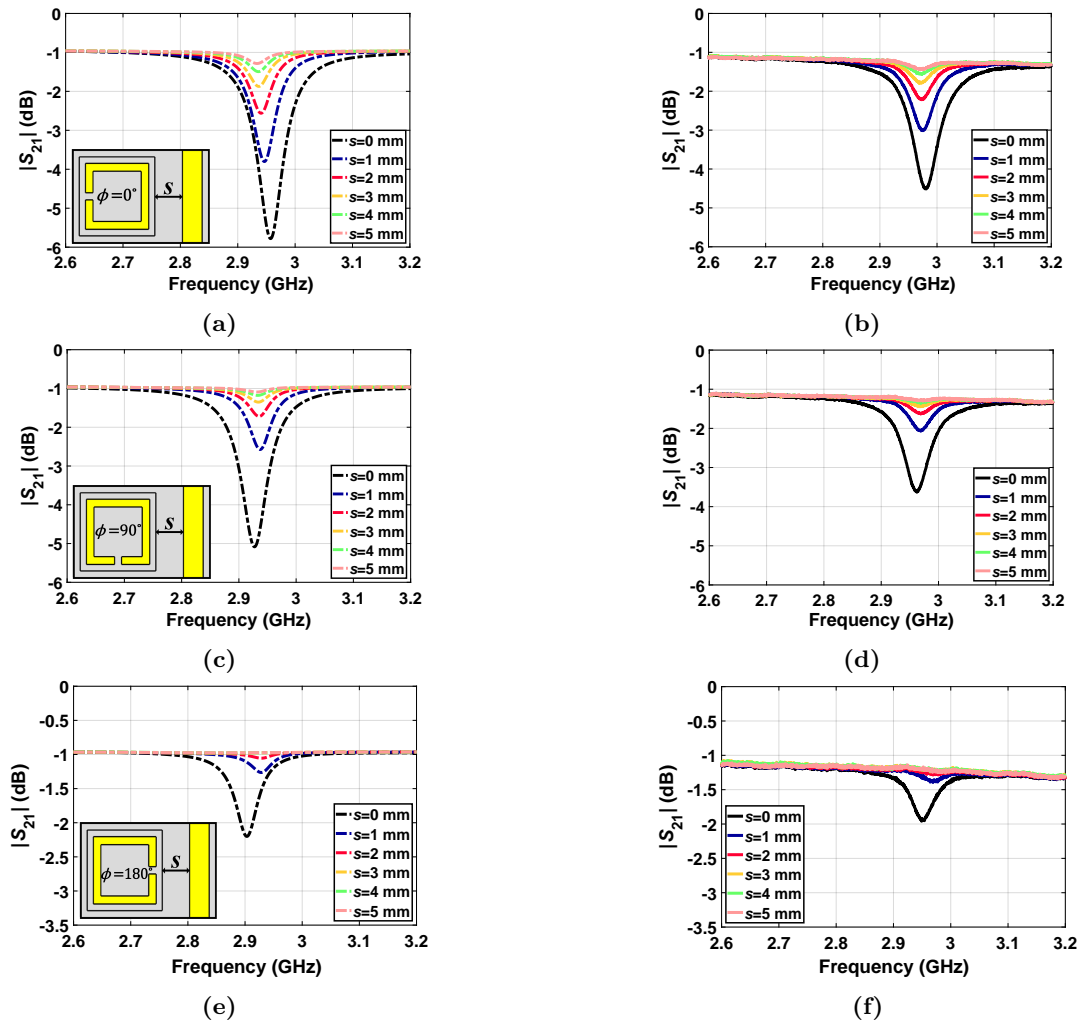


Figure 4. $|S_{21}|$ plots for several s values. (a) $\phi = 0^\circ$ simulation, (b) $\phi = 0^\circ$ experiment, (c) $\phi = 90^\circ$ simulation, (d) $\phi = 90^\circ$ experiment, (e) $\phi = 180^\circ$ simulation, and (f) $\phi = 180^\circ$ experiment. The insets show the SRR shift towards the left for three gap orientation cases.

Secondly, the effects of SRR position on $|S_{21}|$ characteristics were investigated by the parameter s_r for again three gap orientations, where s_r specifies the distance between the reference line and the SRR as depicted in Figures 1 and 5. For that purpose, the SRR was shifted to the right, where s_r was changed from 1 mm to 13 mm with a step-size of 1 mm. The related simulation and experiment results are shown in Figure 5. The white dots in Figure 5 represents the resonance frequency f_0 . Figure 5 reveals that changing s_r both changes f_0 and $|S_{21}|$. Especially for the cases $\phi = 0^\circ$ and $\phi = 180^\circ$, f_0 is highly dependent on s_r . On the other hand, obtaining stronger resonances are possible with changing the value of s_r . For example, in simulations, $|S_{21}|$ value at f_0 for $\phi = 0^\circ$ and $\phi = 180^\circ$ cases reach -10 dB levels, and it reaches to -14 dB level for $\phi = 90^\circ$ case. As observed in Figure 5, the resonance strength reaches its maximum for $\phi = 0^\circ$ at around $s_r = 3$ mm, for $\phi = 90^\circ$ at around $s_r = 3$ mm and $s_r = 11$ mm, and for $\phi = 180^\circ$ at around $s_r = 11$ mm. It was figured out that the coupling between the SRR and the transmission line are the maximum at these specific cases.

Throughout the study, the simulation and the experiment results agree very well. The small discrepancies may be due to fabrication errors, possible errors that may occur during the substrate dielectric property

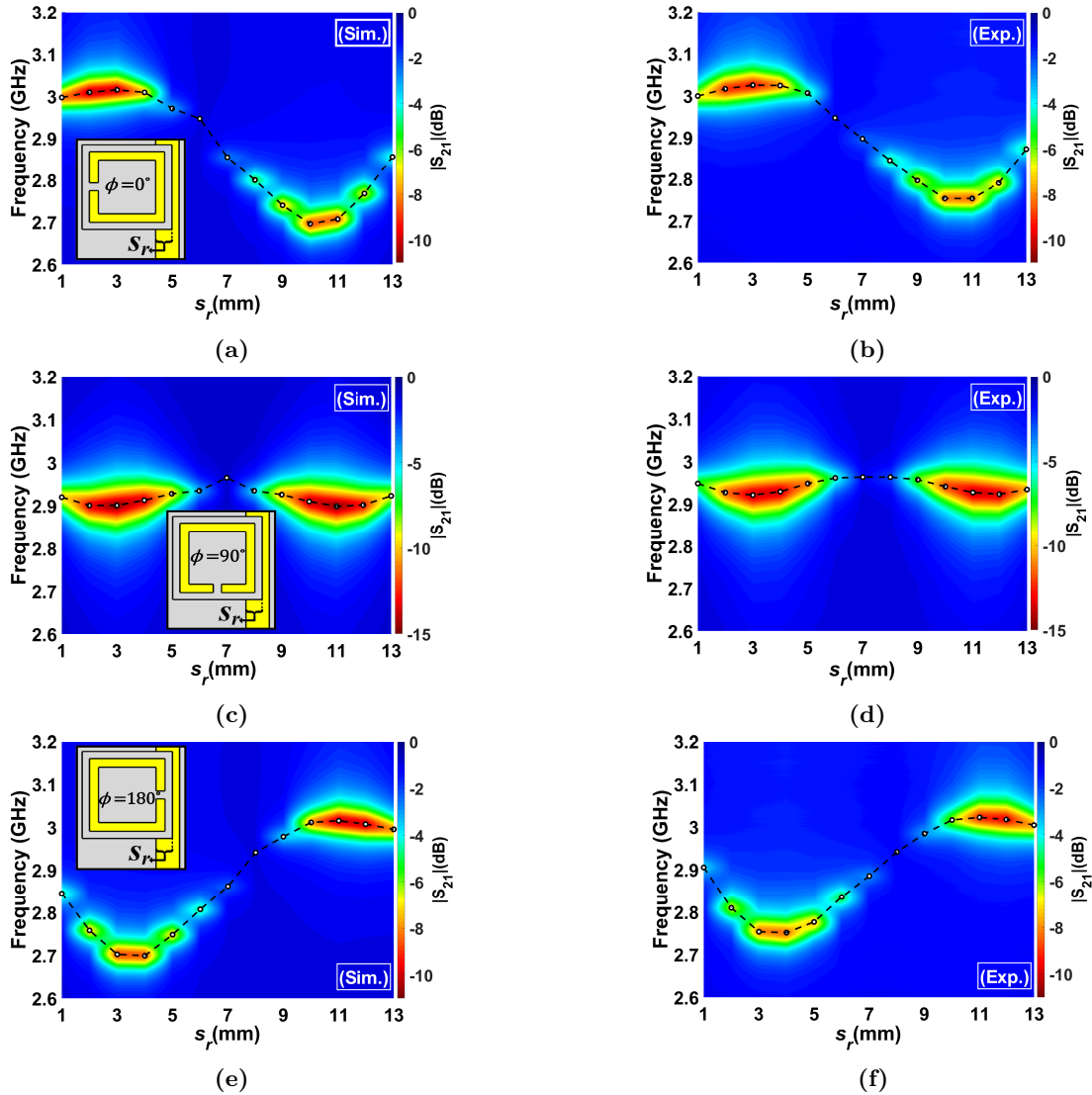


Figure 5. Two-dimensional $|S_{21}|$ graphs and f_0 values for several s_r values and gap orientations. Herein, white dots represent f_0 values. (a) $\phi = 0^\circ$ simulation, (b) $\phi = 0^\circ$ experiment, (c) $\phi = 90^\circ$ simulation, (d) $\phi = 90^\circ$ experiment, (e) $\phi = 180^\circ$ simulation, and (f) $\phi = 180^\circ$ experiment. The insets show the SRR shift towards the right for three gap orientation cases.

retrieval, the unwanted connector/adaptor losses used in the experiments, and tiny errors which may occur in the alignment/positioning of the SRR on the MSTL.

Furthermore, the effects of the thickness of the SRR substrate on the transmission characteristics were investigated for the cases where SRR was positioned on the metallic transmission line. For the analyses, at $s_r = 3$ mm, the SRR substrate thickness h_r was increased from 0.5 mm to 3 mm with a step-size of 0.5 mm without changing the remaining SRR substrate parameters. $s_r = 3$ mm was chosen since it was the shift parameter where the strongest resonances were observed for all gap orientation cases. The simulation results for $\phi = 0^\circ$, 90° and 180° are presented in Figures 6a–6c, respectively. The results show that the $|S_{21}|$ value at f_0 increases (i.e. the resonance strength decreases) as h_r increases for each gap orientation. This is an expected result since the metallic part of the SRR structure moves further and further away vertically from the metallic

transmission line as h_r is increased; therefore, the coupling between the SRR and the MSTL decreases. Not only the amplitude, but also f_0 gets affected in response to increase of h_r for each gap orientation case. For $\phi = 0^\circ$ orientation, f_0 shift to the left up to $h_r = 1.5$ mm, and it shifts to the right after $h_r = 1.5$ mm. For $\phi = 90^\circ$ and 180° orientations, the shift is to the right for all h_r values under investigation. The shift Δf_0 in f_0 is observed to be highest for $\phi = 180^\circ$ and it is lowest for $\phi = 0^\circ$. Besides, Δf_0 decreases when h_r increases for three gap orientation cases. Herein, the responses of f_0 are different in each gap orientation, due to the different coupling mechanisms between the SRR and the MSTL.

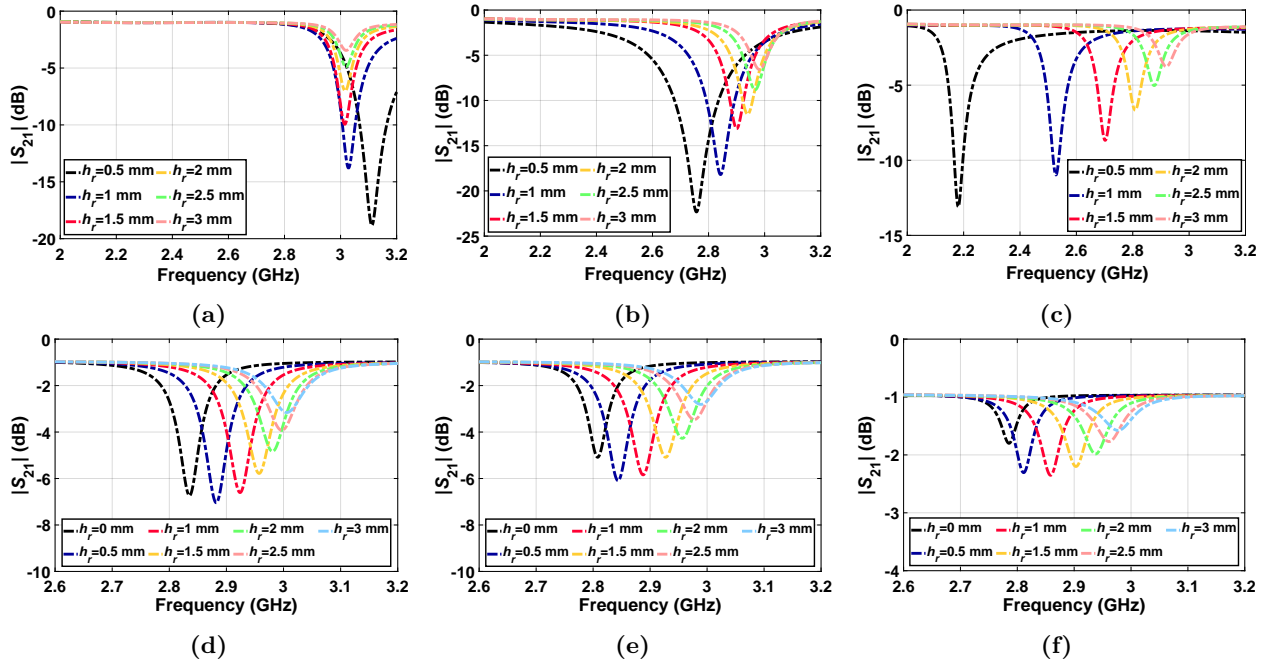


Figure 6. $|S_{21}|$ graphs for several h_r values at $s_r = 3$ mm and for three different gap orientations. (a) $\phi = 0^\circ$, (b) $\phi = 90^\circ$, and (c) $\phi = 180^\circ$. $|S_{21}|$ graphs for several h_r values at $s = 0$ mm and for three different gap orientations. (d) $\phi = 0^\circ$, (e) $\phi = 90^\circ$, and (f) $\phi = 180^\circ$.

To complete the picture, the effects of the thickness of the SRR substrate on the transmission characteristics was also investigated for the cases where SRR was not positioned on the metallic transmission line. For the analyses, the SRR was positioned at $s = 0$ mm, where the resonance strength is the highest, and h_r was increased from 0 mm to 3 mm with a step-size of 0.5 mm again without changing the remaining SRR substrate parameters. The results are shown in Figures 6d–6f for $\phi = 0^\circ$, 90° , and 180° , respectively. In the literature, SRR is commonly positioned co-planarly with the transmission line, i.e. $h_r = 0$ mm [3–14, 21, 23, 24]. However, Figures 6d–6f show that designing the SRR as a separate layer with a nonzero h_r (i.e. for $h_r = 0.5$ mm in Figures 6d and 6e and $h_r = 1$ mm in Figure 6f) increases the resonance strength compared to the $h_r = 0$ mm case. For all three cases, further increase in h_r decreases the resonance strength. On the other hand, increasing h_r increases f_0 . Therefore, designing the SRR as a separate layer provides the flexibility of adjusting its position and gap orientation which may result in tuning the resonance strength and f_0 . These responses may be used in a position sensing application.

Subsequently, the effects of the dielectric constant of the SRR substrate (ϵ_r) on $|S_{21}|$ were investigated. For that purpose, ϵ_r was swept from 2 to 5 with a step-size of 1 for three gap orientations and several substrate thicknesses (i.e. $h_r = 0.5, 1, 1.5, 2, 2.5$, and 3 mm). The simulation results are given in Figure 7. For each gap

orientation, increasing ϵ_r decreased f_0 ; moreover, as h_r increases, the amplitude of $|S_{21}|$ at f_0 is increased for all values of ϵ_r under consideration. In addition, f_0 increases as h_r increases at $\phi = 90^\circ$ and $\phi = 180^\circ$ for all ϵ_r values; however, the increment amount in f_0 reduces as ϵ_r increases. On the other hand, for $\epsilon_r = 2$, f_0 increases as h_r increases and for $\epsilon_r = 3$ and beyond, f_0 firstly decreases then increases at $\phi = 0^\circ$. The results confirm that f_0 and the amplitude of S_{21} both depend on the SRR substrate thickness and the dielectric constant for the three gap orientations.

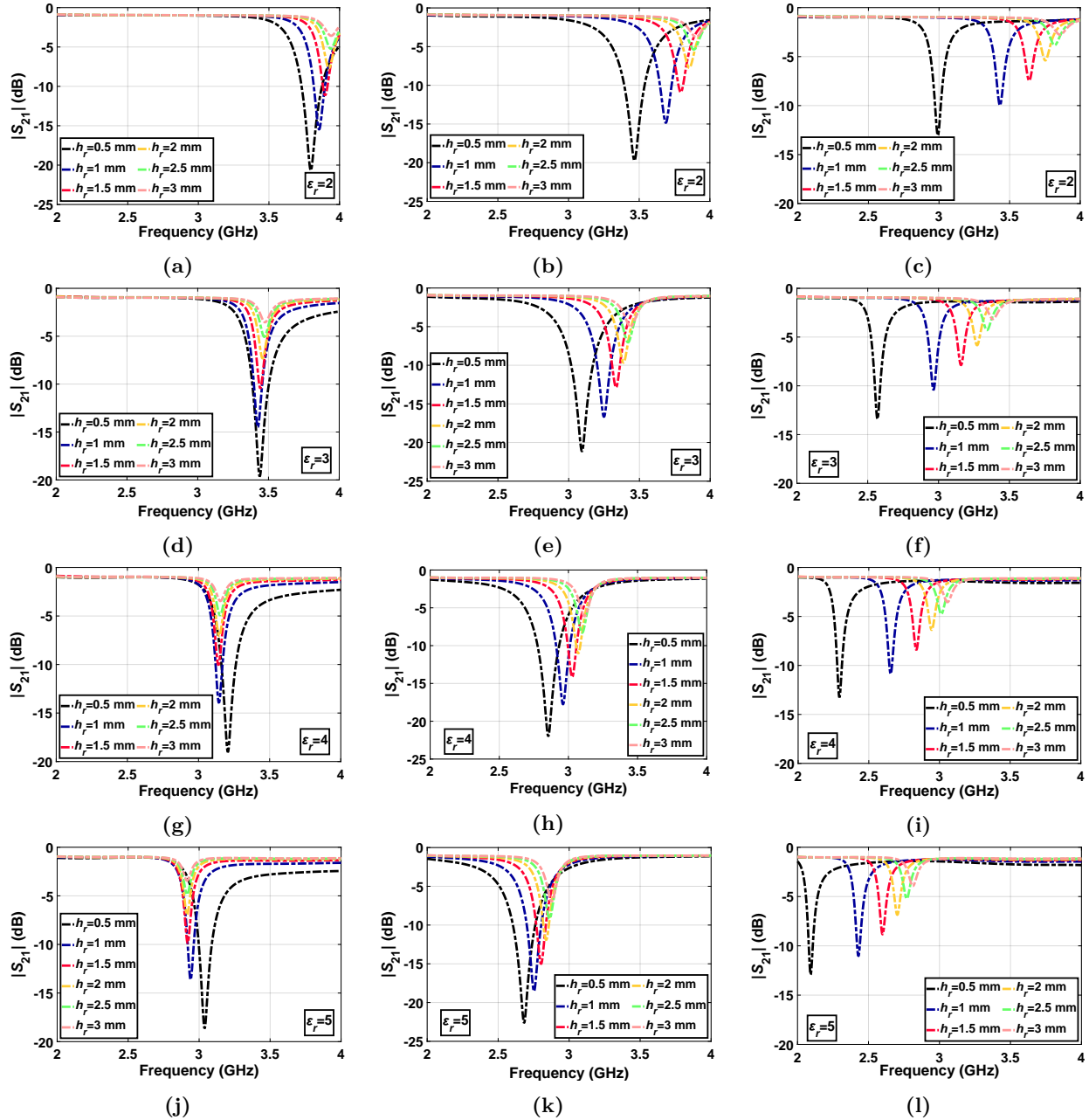


Figure 7. $|S_{21}|$ graphs for various h_r and ϵ_r values at $s_r = 3$ mm for three gap orientations. For $\epsilon_r = 2$ (a) $\phi = 0^\circ$, (b) $\phi = 90^\circ$, and (c) $\phi = 180^\circ$. For $\epsilon_r = 3$ (d) $\phi = 0^\circ$, (e) $\phi = 90^\circ$, and (f) $\phi = 180^\circ$. For $\epsilon_r = 4$ (g) $\phi = 0^\circ$, (h) $\phi = 90^\circ$, and (i) $\phi = 180^\circ$. For $\epsilon_r = 5$ (j) $\phi = 0^\circ$, (k) $\phi = 90^\circ$, and (l) $\phi = 180^\circ$.

Moreover, the effects of gap orientation on the sensitivity, which is important for sensor applications [7, 8, 29], were investigated. For that purpose, the SRR position was kept constant at $s_r = 3$ mm and it was loaded by three different dielectric materials which completely cover the upper surface of the SRR. Hence, the side lengths of the dielectric loadings were $L_s = 11$ mm the thickness were 0.762 mm. The dielectric materials were chosen as Arlon AD255A ($\varepsilon_{diel} = 2.55$ and $\tan\delta = 0.0015$), Arlon AD300A ($\varepsilon_{diel} = 3$ and $\tan\delta = 0.002$) and Arlon AD350A ($\varepsilon_{diel} = 3.5$ and $\tan\delta = 0.003$). The simulation results are shown in Figures 8a–8c. Figure 8 reveals that f_0 decreases in response the dielectric constant increments of the dielectric loadings (ε_{diel}). However, the shifts Δf_0 of f_0 are nearly the same for the three gap orientations. The results show that the choice of gap orientation has no meaningful effect on the sensitivity to dielectric loadings.

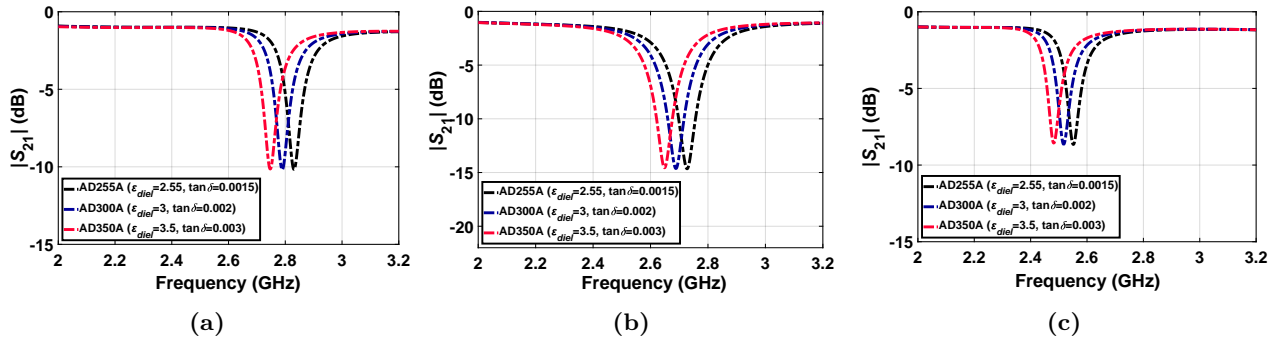


Figure 8. $|S_{21}|$ graphs of SRR structures loaded by Arlon AD255A ($\varepsilon_{diel} = 2.55$ and $\tan\delta = 0.0015$), Arlon AD300A ($\varepsilon_{diel} = 3$ and $\tan\delta = 0.002$) and Arlon AD350A ($\varepsilon_{diel} = 3.5$ and $\tan\delta = 0.003$). (a) $\phi = 0^\circ$, (b) $\phi = 90^\circ$, and (c) $\phi = 180^\circ$. Herein, $s_r = 3$ mm, $h_r = 1.5$ mm, $\varepsilon_r = 4.53$, and $\tan\delta = 0.01$.

Lastly, the power distribution mechanism was examined in simulations for $\phi = 0^\circ$, 90° , and 180° cases at $s_r = 3$ mm and $h_r = 1.5$ mm. In the analyses, to observe the power radiated, the boundaries were terminated by open (add space) boundary conditions. The results are shown in Figure 9. In more detail, the absorption, reflection, and transmission plots for $\phi = 0^\circ$, 90° , and 180° cases are presented in Figures 9a–9c, respectively. The absorption is calculated by $1 - |S_{11}|^2 - |S_{21}|^2$ formula where $|S_{11}|^2$ represents reflectance and $|S_{21}|^2$ transmittance [30, 31]. Herein, the calculated absorption value includes both the dissipated power in the structure, and the power radiated from the structure. In other words, it consists of the dielectric losses, metallic losses, and the radiated power [32, 33]. To confirm that the power distribution plots obtained by CST Studio Suite® are presented in Figures 9d–9f for $\phi = 0^\circ$, 90° , and 180° cases, respectively. In the figures, Power Stimulated refers to the total power at which the overall structure (including the MSTL and the SRR) is excited, the Power Outgoing all Ports refers to the power delivered to the ports (i.e. reflected and transmitted power), Power Accepted refers to the accepted power from the overall structure (regarding dielectric losses, metallic losses, and radiation), Power Radiated refers to the radiated power from the overall structure, and Loss in Dielectrics and Loss in Metals refer to the lost power in the dielectric and metallic inclusions of the overall structure, respectively². In the light of this information, Figures 9d–9f show that some power incident to the overall structure is reflected, some is transmitted, some is dissipated in dielectric and metallic parts, and very little of it is radiated. Finally, antenna gain plots at the corresponding f_0 values are calculated and shown in Figures 9g–9i for $\phi = 0^\circ$, 90° , and 180° cases, respectively. Supporting the low calculated Power Radiated

²CST STUDIO SUITE®, Dassault Systèmes, the 3DEXPERIENCE® Company (online). Website www.3ds.com/products-services/simulia/products/cst-studio-suite/ [accessed 30 December 2021].

values (Figure 9d–9f), the maximum antenna gains are obtained as -4.76 dB, -1.49 dB, and -3.5 dB for $\phi = 0^\circ$, 90° , and 180° cases, respectively. The results show that the designs do not act as radiation elements.

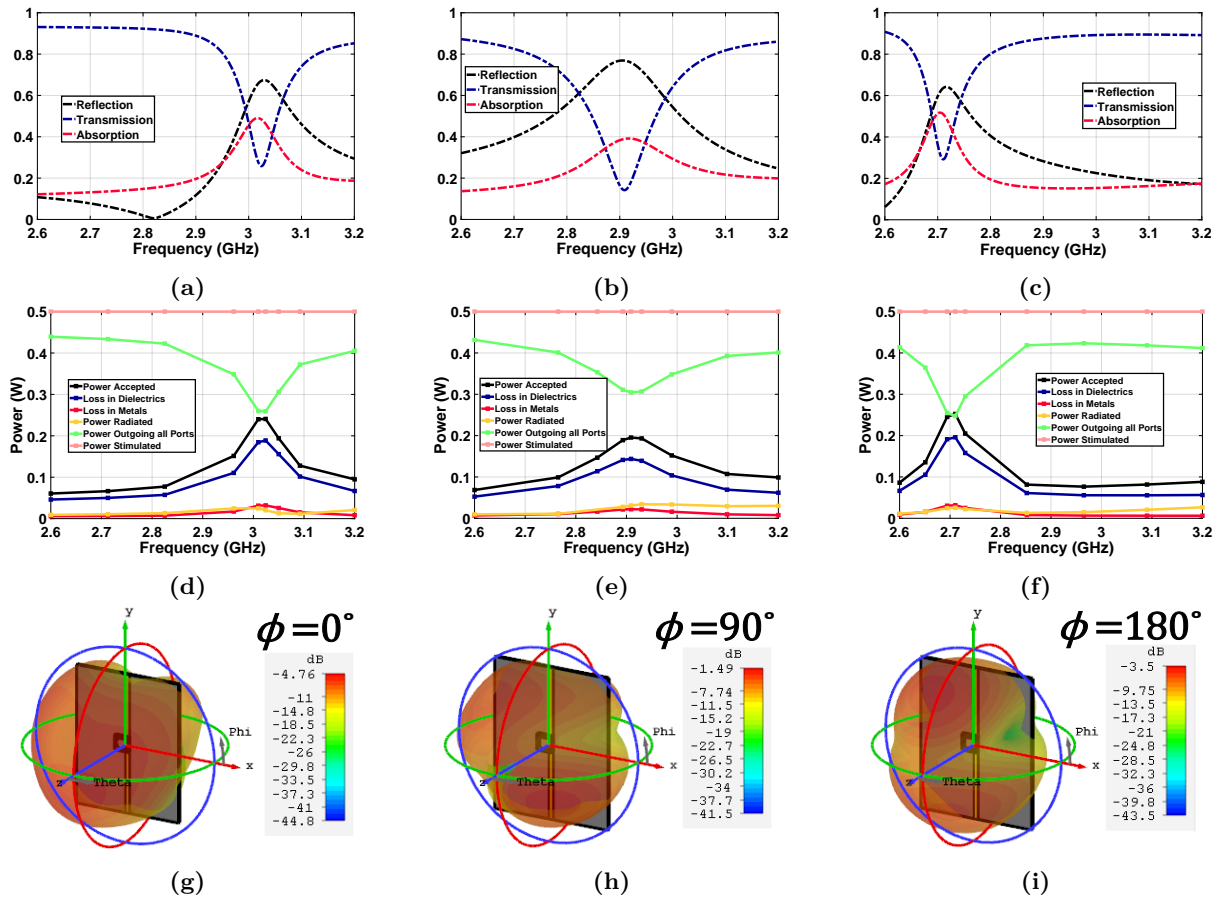


Figure 9. Absorption, reflection, and transmission plots for (a) $\phi = 0^\circ$, (b) $\phi = 90^\circ$, and (c) $\phi = 180^\circ$. Power distribution plots for (d) $\phi = 0^\circ$, (e) $\phi = 90^\circ$, and (f) $\phi = 180^\circ$. Radiation patterns in terms of antenna gain for (g) $\phi = 0^\circ$, (h) $\phi = 90^\circ$, and (i) $\phi = 180^\circ$. Herein, $s_r = 3$ mm, $h_r = 1.5$ mm, $\epsilon_r = 4.53$, and $\tan\delta = 0.01$.

5. Conclusion

In this study, the effects of SRR position and its gap orientation (i.e. $\phi = 0^\circ$, 90° and 180°) with respect to the MSTL on the transmission characteristics are investigated numerically and experimentally. For the first case, it has been observed that the resonance strength decreases as the SRR shift distance to the left (s) increases, while the resonance frequency f_0 is slightly changed. Moreover, the resonance strength decreases as ϕ is increased from 0° to 180° . The resonance even disappears at $\phi = 180^\circ$ for $s = 3$ mm and beyond. In the second case, it has been observed that f_0 and the S_{21} amplitude at f_0 are very sensitive to s_r . During these analyses, stronger resonances have been obtained when the SRR is just above the metallic transmission line due to stronger coupling between the SRR and the MSTL. It has been also revealed by the parametric analyses that the coupling is highly dependent on the SRR substrate thickness h_r . The amplitude of S_{21} at f_0 increases with the increase of h_r for the three gap orientation cases under consideration. Moreover, f_0 has been observed to be highly dependent on the substrate dielectric constant for the three gap orientations. Furthermore, the gap orientation has no meaningful effect on the sensitivity of the SRR in response to the dielectric loadings. Lastly,

the power distribution mechanism has been investigated, and it has been observed that some of the incident power is reflected, some is transmitted, some is dissipated in dielectric and metallic parts, and negligible part is radiated. It has been seen as an important observation that designing the SRR as a separate layer provides a simplicity in terms of adjusting its position and gap orientation, and it may provide an advantage in terms of S_{21} amplitude with a proper setting of h_r value. It is believed that this comprehensive study will be a quick guide for researchers working on sensor and filtering applications whose designs are based on MSTL-loaded resonators.

References

- [1] Veselago VG. The Electrodynamics of substances with simultaneously negative values of ϵ and μ . *Soviet Physics Uspekhi* 1968; 10 (4): 509-514. doi: 10.1070/PU1968v010n04ABEH003699
- [2] Pendry JB, Holden AJ, Robbins DJ, Stewart WJ. Magnetism from conductors and enhanced nonlinear phenomena. *IEEE Transactions on Microwave Theory and Techniques* 1999; 47 (11): 2075-2084. doi:10.1109/22.798002
- [3] Withayachumnankul W, Jaruwongrungssee K, Fumeaux C, Abbott D. Metamaterial-inspired multichannel thin-film sensor. *IEEE Sensors Journal* 2012; 12 (5): 1455-1458. doi:10.1109/JSEN.2011.2173762
- [4] Muhammed Shafi KT, Ansari MAH, Jha AK, Akhtar MJ. Design of SRR-based microwave sensor for characterization of magnetodielectric substrates. *IEEE Microwave and Wireless Components Letters* 2017; 27 (5): 524-526. doi:10.1109/LMWC.2017.2690873
- [5] Saadat-Safa M, Nayyeri V, Khanjarian M, Soleimani M, Ramahi OM. A CSRR-based sensor for full characterization of magneto-dielectric materials. *IEEE Transactions on Microwave Theory and Techniques* 2019; 67 (2): 806-814. doi:10.1109/TMTT.2018.2882826
- [6] Shaterian Z, Horestani AK, Fumeaux C. Rotation sensing based on the symmetry properties of an open-ended microstrip line loaded with a split ring resonator. In: *German Microwave Conference; Nürnberg, Germany: 2015*. pp. 33-35. doi:10.1109/GEMIC.2015.7107745
- [7] Velez P, Munoz J, Mata-Contreras J, Dubuc D, Grenier K et al. Measuring glucose content in aqueous solutions by means of split ring resonator (SRR) loaded transmission lines. In: *12th International Congress on Artificial Materials for Novel Wave Phenomena (Metamaterials); Espoo, Finland: 2018*. pp. 418-420. doi:10.1109/MetaMaterials.2018.8534177
- [8] Kiani S, Rezaei P, Navaei M. Dual-sensing and dual-frequency microwave SRR sensor for liquid samples permittivity detection. *Measurement* 2020; 160: 107805. doi:10.1016/j.measurement.2020.107805
- [9] Withayachumnankul W, Jaruwongrungssee K, Tuantranont A, Fumeaux C, Abbott D. Metamaterial-based microfluidic sensor for dielectric characterization. *Sensors and Actuators A: Physical* 2013; 189: 233-237. doi:10.1016/j.sna.2012.10.027
- [10] Zhang X, Cui WY, Lei Y, Zheng X, Zhang J et al. Spoof localized surface plasmons for sensing applications. *Advanced Materials Technologies* 2021; 6 (4): 2000863. doi:10.1002/admt.202000863
- [11] Zhou H, Hu D, Yang C, Chen C, Ji J et al. Multi-band sensing for dielectric property of chemicals using metamaterial integrated microfluidic sensor. *Scientific Reports* 2018; 8 (1): 14801. doi:10.1038/s41598-018-32827-y
- [12] Talebi N, Shahabadi M, Hafner C. Analysis of a lossy microring using the generalized multipole technique. *Progress In Electromagnetics Research* 2006; 66: 287-299. doi:10.2528/PIER06112801
- [13] Safwat AME, Tretyakov S, Räisänen A. Dual bandstop resonator using combined split ring resonator and defected ground structure. *Microwave and Optical Technology Letters* 2007; 49 (6): 1249-1253. doi:10.1002/mop.22464
- [14] Cinar A, Bicer S. Band-stop filter design based on split ring resonators loaded on the microstrip transmission line for GSM-900 and 2.4 GHz ISM band. *International Advanced Researches and Engineering Journal* 2020; 04 (01): 29-33. doi:10.35860/iarej.641459

- [15] Sun J, Liu L, Dong G, Zhou J. An extremely broad band metamaterial absorber based on destructive interference. *Optics Express* 2011; 19 (22): 21155-21162. doi:10.1364/OE.19.021155
- [16] Islam MR, Islam MT, Moniruzzaman M, Samsuzzaman M, Arshad H. Penta band single negative meta-atom absorber designed on square enclosed star-shaped modified split ring resonator for S-, C-, X- and Ku- bands microwave applications. *Scientific Reports* 2021; 11 (1): 8784. doi:10.1038/s41598-021-87958-6
- [17] Gu J, Singh R, Liu X, Zhang X, Ma Y et al. Active control of electromagnetically induced transparency analogue in terahertz metamaterials. *Nature Communications* 2012; 3 (1): 1151. doi:10.1038/ncomms2153
- [18] Xu N, Manjappa M, Singh R, Zhang W. Tailoring the electromagnetically induced transparency and absorbance in coupled fano-lorentzian metasurfaces: A classical analog of a four-level tripod quantum system. *Advanced Optical Materials* 2016; 4 (8): 1179-1185. doi:10.1002/adom.201600129
- [19] Bie S, Pu S. Array design of 300 GHz dual-band microstrip antenna based on dual-surfaced multiple split-ring resonators. *Sensors* 2021; 21 (14): 4912. doi:10.3390/s21144912
- [20] Chaturvedi D, Raghavan S. SRR-loaded metamaterial-inspired electrically-small monopole antenna. *Progress in Electromagnetics Research C* 2018; 81: 11-19. doi:10.2528/PIERC17101202
- [21] Singh G, Rajni R, Marwaha A. Frequency switching in coupled microstrip line loaded with split-ring resonator. In: *Proceedings of the International Conference on Recent Cognizance in Wireless Communication & Image Processing*; New Delhi, India; 2016.
- [22] Anandan CK, Nimisha CS, Jitha B, Mohanan P, Vasudevan K. Transmission properties of microstrip lines loaded with split ring resonators as superstrate. *Microwave and Optical Technology Letters* 2006; 48 (11): 2280-2282. doi:10.1002/mop.21927
- [23] Rajni, Singh G, Marwaha A. Modeling of split ring resonators loaded microstrip line with different orientations. *International Journal of Electrical and Computer Engineering* 2015; 5 (6): 1363-1371. doi:10.11591/ijece.v5i6.pp1363-1371
- [24] Bojanic R, Milosevic V, Jokanovic B, Medina-Mena F, Mesa F. Enhanced modelling of split-ring resonators couplings in printed circuits. *IEEE Transactions on Microwave Theory and Techniques* 2014; 62 (8): 1605-1615. doi:10.1109/TMTT.2014.2332302
- [25] Karacan N, Bulut NK, Ekmekçi E. Mikroşerit iletim hattı ile uyarılan ayırık halkalı rezonatör yapısının konumunun ve ayırık yöneliminin iletim karakteristiği üzerine etkileri. In: *URSI-TÜRKİYE 2021 X. Bilimsel Kongresi*, Kocaeli, Türkiye; 2021 (in Turkish).
- [26] Nicolson AM, Ross GF. Measurement of the intrinsic properties of materials by time-domain techniques. *IEEE Transactions on Instrumentation and Measurement* 1970; 19 (4): 377-382. doi:10.1109/TIM.1970.4313932
- [27] Weir WB. Automatic measurement of complex dielectric constant and permeability at microwave frequencies. *Proceedings of the IEEE* 1974; 62 (1): 33-36. doi:10.1109/PROC.1974.9382
- [28] Pozar DM. *Microwave Engineering*. Hoboken, NJ, USA: Wiley, 2011.
- [29] Rusni IM, Ismail A, Alhawari ARH, Hamidon M, Yusof NA. An aligned-gap and centered-gap rectangular multiple split ring resonator for dielectric sensing applications. *Sensors* 2014; 14 (7): 13134-13148. doi:10.3390/s140713134
- [30] Tao H, Landy NI, Bingham CM, Zhang X, Averitt RD et al. A metamaterial absorber for the terahertz regime: Design, fabrication and characterization. *Optics Express* 2008; 16 (10): 7181-7188. doi:10.1364/OE.16.007181
- [31] Watts CM, Liu X, Padilla WJ. Metamaterial electromagnetic wave absorbers. *Advanced Materials* 2012; 24 (23): OP98-OP120. doi:10.1002/adma.201200674
- [32] Kajfez D, Guillon P. *Dielectric Resonators*. Norwood, MA: Artech House, 1986.
- [33] Sebastian MT. Measurement of microwave dielectric properties and factors affecting them. In: *Dielectric Materials for Wireless Communication*, 1st ed. Amsterdam, NL: Elsevier, 2008, pp. 11-47.